Atmos. Meas. Tech., 7, 4431–4444, 2014
www.atmos-meas-tech.net/7/4431/2014/
doi:10.5194/amt-7-4431-2014
© Author(s) 2014. CC Attribution 3.0 License.

Atmospheric Measurement Techniques
Open Access

Development of an automated high-temperature valveless injection system for online gas chromatography

N. M. Kreisberg[1], D. R. Worton[1,2], Y. Zhao[2,*], G. Isaacman[2], A. H. Goldstein[2,3], and S. V. Hering[1]

[1]Aerosol Dynamics Inc., Berkeley, CA, USA
[2]Department of Environmental Science, Policy and Management, University of California, Berkeley, CA, USA
[3]Department of Civil and Environmental Engineering, University of California, Berkeley, CA, USA
[*]now at: Department of Chemical Engineering, Carnegie Mellon University, Pittsburgh, PA, USA

Correspondence to: N. M. Kreisberg (nathan@aerosol.us)

Received: 22 May 2014 – Published in Atmos. Meas. Tech. Discuss.: 23 July 2014
Revised: 27 October 2014 – Accepted: 29 October 2014 – Published: 12 December 2014

Abstract. A reliable method of sample introduction is presented for online gas chromatography with a special application to in situ field portable atmospheric sampling instruments. A traditional multi-port valve is replaced with a valveless sample introduction interface that offers the advantage of long-term reliability and stable sample transfer efficiency. An engineering design model is presented and tested that allows customizing this pressure-switching-based device for other applications. Flow model accuracy is within measurement accuracy (1 %) when parameters are tuned for an ambient-pressure detector and 15 % accurate when applied to a vacuum-based detector. Laboratory comparisons made between the two methods of sample introduction using a thermal desorption aerosol gas chromatograph (TAG) show that the new interface has approximately 3 times greater reproducibility maintained over the equivalent of a week of continuous sampling. Field performance results for two versions of the valveless interface used in the in situ instrument demonstrate typically less than 2 % week^{-1} response trending and a zero failure rate during field deployments ranging up to 4 weeks of continuous sampling. Extension of the valveless interface to dual collection cells is presented with less than 3 % cell-to-cell carryover.

1 Introduction

In the atmosphere, organic compounds play a central role in the processes that generate tropospheric ozone and secondary organic aerosol (SOA). Many thousands of these organic compounds have been identified in both the gas and particle phases (Hamilton et al., 2004; Lewis et al., 2000) using various chromatographic techniques, including gas chromatography (GC), and these most likely represent only a small fraction of what is actually present (Goldstein and Galbally, 2007). It is important to characterize and quantify this atmospheric pool of volatile, semi-volatile, and non-volatile organics in order to improve our understanding of ozone photochemistry and SOA formation.

Since the majority of these organic compounds are present in the atmosphere in low abundance, sample concentration prior to analysis is necessary. This pre-concentration can be performed in a variety of ways, e.g., adsorbent traps, impactors, or filters (Ras et al., 2009; Williams et al., 2006; Zhao et al., 2013a), depending on which organic species are of interest and whether they are in the gaseous or condensed phases. For semi-continuous in situ measurements, the analysis and sampling are ideally conducted simultaneously to minimize gaps in measurement. Regardless of the collection method employed, the pre-concentration sampling inlet should be isolated from the analysis components of the instrument. This separation is often achieved using a two-position, six-port valve.

Recently, there has been an increased focus on the identification and quantification of low-volatility compounds in the atmosphere, with vapor pressures less than ~ 50 Pa (equivalent to n-dodecane at 20 °C), especially with respect to their role as precursors to SOA (Robinson et al., 2007; Kroll and Seinfeld, 2008). Efficient transfer of these compounds from a collection cell to the detector requires high-temperature

transfer lines. Any switching valve employed in the sample transfer path must also be similarly heated. The presence of mechanical seals imposes a maximum temperature (∼ 300 °C) for the valve. Further, wetted polymeric composite seals (e.g., polyamide/graphite) within a valve contribute to incomplete sample transfer of more polar compounds. Mechanical switching inevitably leads to a risk of leaking, sample degradation, and loss, which ultimately requires valve rotor replacement, leading to instrument downtime. In GC applications, leaks contribute to column stationary phase decomposition and degradation of the chromatography. Further, when a mass spectrometer is employed, these leaks can cause oxidation of the ion source, shortened electron impact filament lifespan, and reduced sensitivity. To significantly reduce such problems and to improve the reliability and long-term instrument stability, we sought a suitable substitute for the classical sample injection valve.

In this work, we replaced the two-position, six-port valve (Valco Instruments Co. Inc) on our thermal desorption aerosol gas chromatograph (TAG) instrument with a novel valveless injection (VLI) system. Although it was arrived at independently, the fundamental design of the VLI system described here is a natural extension of the early pressure switching work of Deans (1972, 1973, 1984a, b), who argued that with such a design one could maximize transfer efficiency and increase reproducibility and reliability at the same time. TAG is an in situ instrument for the hourly measurement of organic compounds in atmospheric aerosols. Samples are collected for approximately 30 min and then immediately transferred via thermal desorption onto a gas chromatograph. The chromatographic analysis is conducted during the collection of the subsequent sample, as described in more detail by Williams et al. (2006). The reliability of using this heated valve on the TAG instrument has been highly variable, with observed rotor seal lifetimes ranging from immediate failure, likely stemming from operating in a dirty environment, to several months. The application of an anti-stiction coating (AMC-18, Advanced Materials Components Express, Lemont, PA) to the rotor appears to reduce wear and extend the lifespan significantly (B. J. Williams, personal communication, 2014), but quantifying this improvement would be difficult and prohibitively time consuming. As a result of valve seal failures, there were periods of instrument downtime during in situ sampling when measurements were not possible, resulting in prolonged gaps in an otherwise continuous data set.

Here two versions of the VLI are presented: the original discrete-component prototype VLI system and an improved, integrated-manifold version. A design model of the VLI flows is presented, and its accuracy is evaluated through direct laboratory measurements. The performance of the discrete-component prototype VLI was evaluated in the laboratory with direct comparison to the six-port valve of the original TAG. Both versions of the VLI have been deployed in field studies, and data are presented here to demonstrate reliability of the interface and the degree of consistency in sample delivery obtained while operating in challenging environments. Extension to the transfer of highly polar compounds using online derivatization and the adaptation of the integrated-manifold VLI to a dual-cell system for simultaneous paired sample collection is demonstrated.

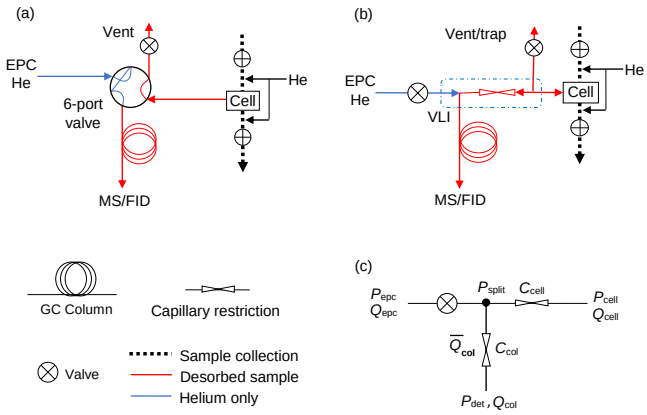

Figure 1. Flow diagrams shown in sampling/analysis mode for **(a)** original sample injection system employing a dual-position, six-port valve and **(b)** valveless injection system showing metal capillary tubing constrictions in conjunction with the GC silica capillary tubing for flow regulation. Flow direction (arrows), magnitude (thickness), and sample transfer lines (red) are indicated for each path in sampling/analysis mode. **(c)** Simplified diagram of valveless system showing pressure reading points P_x used for modeling the flows Q_x in capillaries C_x where the vent and cell have been treated as one leg. During sample injection, the six-port valve connects the cell to the column **(a)**, while in the valveless system **(b)** the pressurized cell reverses flow Q_{cell} to direct the desorbing sample onto the column.

2 Valveless interface (VLI) design and modeling

2.1 Generic system description

An online chromatographic instrument for continuous operation requires a method of repeatedly introducing samples into the analysis section by coupling two independent flow subsystems – the sample collector and the gas chromatograph – and conveying the concentrated sample ultimately to the head of the analytical column. The VLI system is a pressure-balancing, split-flow method that employs a restrictive capillary tube between the collection cell and the inlet of the chromatograph. The capillary flows have been modeled in the context of a gas-chromatography-based system, but the mathematical approach allows adaptation for different applications, e.g., alternate collection techniques or GC column sets or stand-alone detectors with a suitable inlet restriction replacing the GC column.

Figure 1 shows a schematic of the original method of sample injection using a six-port valve (a) and the VLI system (b)

when employed with a sampling system consisting of a single collection and thermal desorption (CTD) cell. During aerosol collection, the sampling valves located on either side of the CTD cell are open, and a vacuum pump pulls the atmospheric sample into the cell at approximately 10 L min^{-1}. Depending on the design of the CTD, the pressure within the cell during sampling, P_{cell}, is between ~ 50 and 95 kPa (Williams et al., 2006; Zhao et al., 2013a). Simultaneously with sample collection, the gas chromatograph is operated to analyze the previously collected sample. In contrast to the relatively large sample collection rate, the GC operates with open tubular capillary flows on the order of 1 mL min^{-1} (usually helium as carrier gas), and the pressure at the head of the column (P_{split}) is on the order of 300 kPa. This large flow differential between sampling and analytic flows facilitates an open connection between them if done with a suitably restrictive means that permits flow direction reversal under pressure control. Either an orifice or small bore capillary tubing can be used for such a restrictive passage, but extended capillary tubing provides more reliable performance and greater flexibility since the tube length approximates a continuously tuneable linear parameter and larger bores are less susceptible to clogging. The vent valve provides the option for purging the CTD cell with carrier gas prior to injection.

Two flow states are used during operation of the TAG instrument: (1) concurrent collection and analysis ("load"), wherein excess helium carrier gas flow over that required for the column is bled into the CTD cell, and (2) sample transfer from the cell to the column ("inject") is conveyed by a second helium source. During sampling, concurrent with analysis of the prior sample, a small flow of helium flows from the split point into the CTD cell. This flow is typically < 0.1 % of the sampling flow rate of the TAG instrument and thus requires no correction to sample volumes. Conversely, during sample transfer, valves on either side of the cell and the vent are closed, and the auxiliary helium source at fixed pressure P_{CTD} drives the desorbed sample to flow onto the head of the column. During this transfer period, the flow delivered by the electronic pressure controller (EPC), Q_{epc}, is either shut off via a solenoid valve or set to a minimum to allow maximum transfer rates from the CTD cell to the column while avoiding any sample diversion at the split point (P_{split}). To enable the use of a small constant purge flow from the EPC during injection, an additional restrictive capillary, C_{epc}, replaces the valve as discussed further in Appendix A. A mass flow controller on the CTD cell regulates the flow through the cell during the purge and cell cooldown steps, when the CTD cell is vented to the atmosphere. Originally, the vent was used to purge water present with cool-down atmospheric aerosols (Williams et al., 2006) and to purge solvent following injection of a liquid standard (Kreisberg et al., 2009).

A variation of this scenario involves the addition of a secondary focusing trap on the vent path that enables the use of higher, more efficient desorption flow rates through the cell than can be achieved with direct injections onto a restrictive GC column (Zhao et al., 2013a). After the cell is completely desorbed, the vent valve is closed and a secondary helium purge control valve is opened to back-flush the trapped sample rapidly onto the column at 1–4 mL min^{-1} flow rates. The secondary focusing trap offers the further advantages of (1) increasing sample volatility from reduced cell pressure (i.e., lowers boiling points of analytes) and (2) avoiding introduction of potentially harmful reagents to the analytic column when employing online derivatization methods (Isaacman et al., 2014). The secondary focusing trap is used on the vent line of the SVTAG instrument employing the filter-based sampler cell (Instrument 2 defined below), while the original impactor-based instrument did not have this component (Instrument 1 defined below).

2.2 Gas flow model

The pressure-drop-dependent flows of each of the capillaries used to build a valveless interface have been modeled, and operational control stems from manipulation of the carrier gas head pressure (P_{epc}) and the sample collection cell pressure (P_{cell}). For typical constant-flow GC operations, P_{epc} increases with the oven temperature in a programmed way to provide a constant flow of carrier gas onto the column during analysis (Blumberg, 2010).

With an assumed ideal gas behavior, the carrier flow within the injection system can be modeled exactly with governing expressions derived algebraically. The expressions we derive are in the most general way to facilitate adaptation to other applications. The custom hardware employed is described, but off-the-shelf parts can be used, as with our prototype, without significant compromise for other applications (e.g., see Appendix A).

The volumetric flow governs transport of analytes out of the collection cell (at cell temperature and pressure (T, P) conditions) during desorption and through the column itself during analysis per standard chromatography theory (e.g., McNair and Miller, 2011). Key to a correct formulation is consistent use of the appropriate temperature and pressure references as dictated by mass flow conservation and the ideal gas approximation. Turbulence, non-continuum, entrance, and wall effects are assumed to be negligible and otherwise become subsumed in the capillary calibration process as described in the next section. These physical conditions are broadly satisfied with gas chromatography (Blumberg, 2010).

We present the theory of operation for the simpler interface configuration that uses a valve on the carrier gas line as shown in Fig. 1. The original, more general configuration uses an additional flow control capillary instead of this valve and was used in the prototype. The theory of operation for this more general approach is presented in Appendix A. Both ambient-pressure- and vacuum-based detectors are considered such as a flame ionization detector (FID) and mass spectrometer (MS), respectively. Using vacuum outlet condi-

tions appropriate for mass-spectrometer-based detection not only simplifies the formulation but also offers better chromatographic performance over ambient pressure detectors when operating near optimum GC capillary column conditions (Giddings, 1964).

Referring to Fig. 1c, the pressure at the head of the column, P_{split}, determines the flow to and from the cell and through the column in conjunction with P_{cell} and P_{det}, respectively. The carrier gas source pressure at the EPC equals the split pressure ($P_{epc} = P_{split}$) when the valve on the EPC line is open and minimally restrictive tubing is used for that pathway. The case in which this tubing is intentionally made restrictive and therefore $P_{epc} \neq P_{split}$ is covered in Appendix A. The pressure at the detector is taken as fixed either at 101 kPa for an atmospheric-pressure-based detector (e.g., FID) or at 0 kPa for a mass spectrometer. Thus variations in the flow of carrier gas through the column are determined by variations in the pressure at P_{split} alone. Flow rates and direction between the CTD cell and the split point are controlled by the relative pressure $P_{split} - P_{cell}$.

For the pressure drops normally encountered with gas chromatography, modeling the pressure and flow in the VLI capillaries, including the chromatograph column, calls for use of the compressible Hagen–Poiseuille equation (Blumberg, 2010). The form of this equation relates the capillary outlet flow Q_o to a given inlet pressure P_i and outlet pressure P_o given the temperature-dependent carrier gas viscosity $\eta(T)$, capillary length L, internal diameter d, and temperature T:

$$Q_o = \left(\frac{\pi d^4}{256\eta(T)L}\right)\left(\frac{P_i^2 - P_o^2}{P_{ref}}\right)\left(\frac{T_{ref}}{T}\right). \quad (1)$$

Flows are evaluated at reference conditions T_{ref} and P_{ref}, e.g., 298 K and 101 kPa for ambient outlets, and the entire length of the capillary is assumed to be at temperature T. The temperature dependence of helium's dynamic viscosity can be conveniently predicted with 0.2 % accuracy over the temperature range of 300–700 K based on a least-squares fit to standard reference data (Lide, 1991) by the relation

$$\eta(T) = 2.003 \times 10^{-5} \cdot (T/T_0)^{0.695} \quad (2)$$

in Pa s with T in K and $T_0 = 303.15$ K. Similar expressions can be found for other carrier gases.

For analysis mode, the goal is to obtain an equation defining the controlling parameter, namely $P_{epc}(= P_{split})$, in terms of the input parameters P_{cell}, P_{det}, T_1, T_2, and T_{col} and the desired column flow. Two options are available for specifying the column flow: (i) as an outlet flow given by Eq. (1) at a specific reference condition such as standard pressure and temperature or (ii) the average flow may be desired, requiring the use of the compressibility factor j_c (James and Martin, 1952; Davankov et al., 1999) that relates the average pressure in a capillary relative to the outlet pressure P_o through $\bar{P} = P_o / j_c$, where

$$j_c = \frac{3\left(P_i/P_o\right)^3 - 1}{2\left(P_i/P_o\right)^2 - 1}. \quad (3)$$

Using (T_{col}) for the reference conditions in Eq. (1) gives an expression for the average column flow rate as

$$\bar{Q}_{col} = \frac{3a_{col}\left(P_{split}^2 - P_{det}^2\right)^2}{2\left(P_{split}^3 - P_{det}^3\right)}, \quad (4)$$

where a capillary conductance factor is introduced as $a_{col} = \pi d_{col}^4[256\eta(T_{col})L_{col}]^{-1} a_{col} = \pi d_{col}^4[256\eta(T_{col})L_{col}]^{-1}$.

For the case of a vacuum-based detector where $P_{det} = 0$, Eqs. (1) and (4) simplify greatly to obtain closed-form expressions solvable for P_{split} in terms of a desired outlet or average column flow. For other outlet conditions, these equations can be solved numerically.

During sample injection, the EPC valve is closed and the pressure in the cell is set to a maximum (or the outlet of a focusing trap if employed during its back-flushing) to drive the thermally desorbing sample at the highest allowable flow rate onto the head of the column where it re-condenses prior to GC analysis. This injection flow rate is to first approximation given by Eq. (1), with $P_i = P_{cell}$ and outlet pressure $P_o = P_{det}$, because the column restriction is much greater than the VLI capillary (i.e., $a_{cell} \ll a_{col}$). Knowledge of the exact injection flow rate is only used with the GC application when judging potential line leaks since this flow can be monitored via a mass flow controller. In a situation where this injection flow is used for immediate detection, a more accurate estimate for the flow can be determined by including the small contribution from a_{cell} into an effective conductance factor a'_{col}.

2.3 Prototype VLI

The VLI prototype built with discrete components is shown in Fig. 2a and represents the configuration shown in Fig. 1b. A 50 cm long stainless-steel capillary with inner diameter (ID) of nominally 125 µm (Upchurch, WA, USA) was connected by a pair of zero dead volume tees (Valco Instruments Co. Inc., Houston, TX, USA). Instead of using a valve to shut off the EPC flow, as shown in Fig. 1c, a second capillary identical to C_{cell} substituted for this valve. This complication produces negligible sample redirection during injection by virtue of a steady but small purge flow maintained out of the EPC. Further discussion of the reasons for this substitution are detailed in Appendix A in addition to the method used to program the EPC when $P_{split} \neq P_{epc}$.

The prototype was housed in a machined aluminum block enclosure maintained at 300 °C with a pair of steel stand-offs to rest on top of the GC oven. An outer sheet metal enclosure, not shown, holds a layer of insulation surrounding the

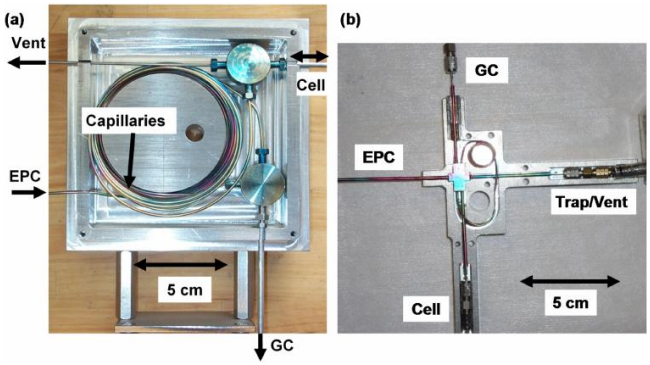

Figure 2. (a) Prototype valveless system using discrete components including a pair of zero dead volume tees and two capillary coils. **(b)** Integrated capillary manifold version of the VLI replaces the discrete tees with a miniature bored manifold into which five capillaries are permanently brazed. The control capillary is seen as a coiled loop connecting one side of each interior tee.

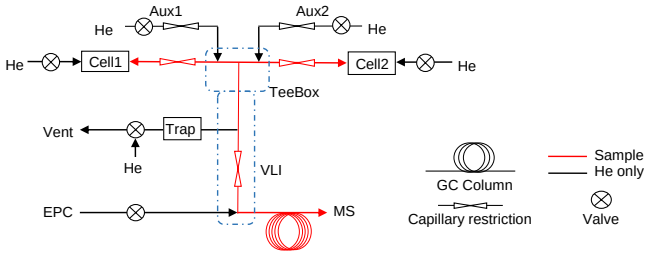

Figure 3. Modified valveless injection scheme incorporating two parallel sampling cells to be analyzed sequentially after the samples are initially transferred to a secondary focusing trap. Auxiliary purge valves (Aux1 and Aux2) are used to avoid cross transfer of sample between parallel cells. Dashed squares delineate integrated VLI manifold and a separate heated box for the additional tees ("TeeBox"). Atmospheric sampling lines for both CTD cells are omitted for clarity.

inner heated box. To provide uniform temperatures, the capillaries were wound around an 8 cm diameter, 2.5 cm thick central hub into which both the cartridge heater and a thermocouple were inserted for use with a temperature controller. Slots in the walls allow passage of 1/16 in. outer diameter (OD) connecting capillaries. Also shown are 6 mm OD aluminum rods grooved to hold the capillaries needing continuous heating, namely those from the cell and to the GC, captured in the wall of the box to transfer heat. To minimize sample losses during thermal desorption, all stainless steel capillaries and tees were chemically passivated (Inertium® treatment, AMCX, PA, USA).

2.4 Integrated VLI

Following the successful first field deployment of the prototype VLI, an improved version of the interface was designed with the goal of reducing the number of compression fittings and total thermal mass to provide further increases in performance and reliability. The design of the modified VLI, shown in Fig. 2b, replaces the two discrete tees with a single miniature flow manifold (13 mm × 9.5 mm × 3.2 mm) machined from a single block of stainless steel. The restrictive capillary tubing (C_{cell} in Fig. 1c) consists of a coiled 30 cm long × 0.8 mm OD × 0.12 mm ID tube brazed into two ports of the manifold. The remaining ports are typically made from 5 cm long × 1.6 mm OD × 0.25 mm ID pre-cut tubes (Upchurch). A compact, conforming aluminum block (Fig. 2b inset) was machined to enclose the manifold, including cavities to enclose miniature compression fittings used to make external connections (e.g., SilTite, SGE, TX, USA). Aluminum rods (6 mm OD) machined with lengthwise slots provide continuous heating for all sample handling transfer line tubing with outer diameters of 1.6 or 0.8 mm. This integrated version is now in use on multiple versions of the TAG instrument, including the recently developed combined TAG and aerosol mass spectrometer (TAG–AMS) hybrid instrument (Williams et al., 2014). A normally open instrument grade solenoid valve (411 series, ASCO) is used to shut off the EPC flow during injection. Other than the pressure set point formulation, no significant difference exists between the two versions of the VLI, and they would be expected to perform similarly.

2.5 Dual-cell modification

A further modification was made to the integrated manifold VLI to expand the capabilities of the semi-volatile targeted thermal desorption aerosol gas chromatograph (SV-TAG) by including a second parallel sampling cell for gas–particle partitioning studies. This dual-cell system uses an expanded valveless interface as described here, while further details including the sampling methodology may be found elsewhere (Isaacman et al., 2014). The addition of two auxiliary purging lines provides a means to selectively inject the thermal desorption flow from either one of two collection cells as shown in Fig. 3. For example, during the thermal desorption of CTD2 the auxiliary purge valve Aux1 is opened to release helium into the collected output of three tees ("TeeBox") to prevent thermal desorption flow out of CTD2 from entering CTD1. This minor purge flow first pressurizes the non-desorbing cell before combining with the other cell's desorption flow to fully sweep the sample out to the focusing trap. The additional purge flow slightly increases (< 20 %) the total desorption flow conveying the sample to the trap. Higher desorption flows through the focusing trap reduce the focusing trap's efficiency for the lightest compounds analyzed, but small reductions in the trap temperature (< 5 °C) can more than compensate for these losses (Zhao et al., 2013a). Passive flow balancing of the purge lines is achieved using measured lengths of 0.25 mm ID capillary tubing in the ratio of desired flow split.

3 Laboratory and field testing methods

3.1 Measuring modeled flows

To test the governing control theory models, a discrete version of the VLI was used to measure capillary flows as a function of inlet and outlet pressures and temperature. An absolute pressure gauge was temporarily inserted at the split point to directly measure P_{split}. The column and vent flow were measured as a function of capillary temperature and the pressures at the inlet and outlet. The vent flow is equivalent to the maximum flow that can enter the cell during sampling when the vent is closed. The range of control parameters used represents typical ranges encountered in TAG-based applications of the VLI: 30–300 °C for the GC column, 300 °C isothermal for the VLI interface components, 140 to 430 kPa absolute inlet pressure, and either 101 or 0 kPa absolute outlet pressure.

Capillary volumetric flows were measured either directly at the outlet or indirectly through timed column transit times of non-retained gas injections to the mass spectrometer. The Q_{epc} outlet flow was measured on the vent line, Fig. 1b, with the cell sampling valves closed using a volumetric flow bubble meter (Gilibrator, Sensidyne, FL, USA) with a 1 % specified accuracy. For column outlet flow at ambient condition (FID detector), a graduated pipette-based soap bubble meter was used with stopwatch-timed transits. The volume of the pipette was confirmed using water and a gravimetric scale. The largest source of error is in the manual timing of bubble transits, so an empirical estimate of uncertainty was obtained from triplet measurements of 25 flow rate readings over the range of 1.7 to 20 mL min^{-1}. The mean relative standard deviation of 1 % was taken as the uncertainty of these flow rate measurements.

For the vacuum outlet case, the average volumetric column flow given by Eq. (4) was determined indirectly through measured transit times of non-retained gas injections passing through the column and detected by the mass spectrometer. A septum port was temporarily introduced immediately upstream of the capillary split point (P_{split} in Fig. 1) to introduce syringe-based injections of air with volume ~ 1 µL at ambient pressure. Silica capillary tubing used for gas chromatography columns is manufactured with strict process controls resulting in very tight tolerances on internal diameter. The manufacturer's internal diameter (0.25 mm) was used to calculate the silica column's internal volume to be 1.47 cm^3. The additional dead volume introduced with the temporary injection port was estimated to be 0.12 cm^3 or less than 10 % of the column volume. No corrections to capillary dimensions were made for temperature expansion because the change in fused quartz dimensions for a 300 °C operating range is less than 0.02 %.

3.2 Comparing prototype VLI to six-port valve

Performance of the prototype VLI system was evaluated using measurements of sample transfer performance over the course of months during development of the SV-TAG, a version of the in situ thermal desorption aerosol gas chromatograph targeting semi-volatile atmospheric organics (Zhao et al., 2013a). Sample injection stability was judged by use of manual 5 µL injections of authentic standards directly into the CTD cell through a built-in injection port (Kreisberg et al., 2009). Samples were analyzed using standard GC–MS methods as detailed elsewhere (Williams et al., 2006; Zhao et al., 2013a). Laboratory evaluations comparing the VLI performance relative to the original six-port valve were conducted using injected standards of a complete suite of even *n*-alkanes from C_8 to C_{40} (Accustandard). Two 1-month periods of laboratory measurements are compared that approximate continuous field operation on each of the two injection systems. Sample transfer variability was evaluated through the relative recovery of *n*-alkanes by normalizing each compound's peak area response by that of eicosane's (C_{20}). Long-term stability is best judged this way because absolute variability from manual injections can be greatly reduced using automated injection systems (Isaacman et al., 2011) and changes in detector response or "drift" are removed through internal standard corrections (Worton et al., 2012). In particular, loss in transfer efficiency for compounds with the lowest volatility (largest number of carbon atoms) serves as the most sensitive indicator of reduced sample transfer efficiency for the case of a fixed sample matrix such as in using injected standards alone.

3.3 Evaluating VLI field performance

The VLI field performance is illustrated with two versions of the TAG instrument. The first, hereafter referred to as Instrument 1, introduced the prototype version of the VLI along with a vapor-phase denuder for the study of gas–particle partitioning (Zhao et al., 2013b). Instrument 1 was deployed during the Research in California at the Nexus of Air Quality and Climate Change (CalNex) campaign from 31 May to 27 June 2010. Ambient samples were acquired at 9 L min^{-1} for two durations: 90 min from 31 May to 9 June and 30 min from 10 to 27 June. Further details of the sample collection and analysis can be found elsewhere (Zhao et al., 2013b). Field-based evaluations of the VLI performance during this study were based on the use of perdeuterated internal standards (*n*-alkanes and poly aromatic hydrocarbons; C/D/N Isotopes) manually injected on top of ambient samples at an average rate of 1.6 per day throughout the 29 days of continuous sampling. Injections were performed as described above. The recovery of internal standards allows corrections to be made in the quantification of ambient compound peaks from factors such as changing detector response or changes in sample transfer driven by variable sample matrices (Wor-

ton et al., 2012; Lambe et al., 2009). Under relatively stable ambient concentrations and detector response, recovery of internal standards serves as an absolute stability test of the whole thermal desorption process including the VLI. Since the more volatile, non-polar internal standards have reduced sample matrix sensitivity, they are a more reliable indicator of short-term stability in transfer efficiency when a changing sample matrix exists. To evaluate the transfer efficiency of the TAG during the study, relative responses are presented for all internal standard hydrocarbons more volatile than *n*-dotriacontane (C_{32}).

A second version of the TAG, Instrument 2, used the integrated manifold version of the VLI and was further modified for online derivatization using two parallel sampling cells, as detailed elsewhere (Isaacman et al., 2014). The VLI was extended to allow independent introduction of samples from each cell to perform serial analysis for pairs of samples acquired in parallel (usually one through a denuder and one directly) as shown in Fig. 3. Unlike prior versions of the TAG, this version of the instrument collects samples in a thermally regenerated metal fiber filter cell designed to capture semi-volatile compounds in the vapor phase with high efficiency (Zhao et al., 2013a). Recent field measurements in rural Brazil with Instrument 2 allow evaluating the integrated VLI for a wide range of compounds in a region influenced by both tropical rain forests and intermittent urban emissions. With the newly introduced online derivatization, the stability of the integrated VLI was evaluated using automated injections of a suite of internal standards injected on top of every ambient sample acquired during continuous sampling from 27 February–18 March 2014 at $10\,\mathrm{L\,min^{-1}}$ for a pair of simultaneous 20 min samples on the two cells. The internal standards used included: perdeuterated C_{14}–C_{32} *n*-alkanes (even carbon numbers only), decanoic acid–d_{19}, tetradecanoic acid–d_{27}, hexadecanoic acid–d_{31}, octadecanoic acid–d_{35}, pentadecanol–d_{31}, cholesterol–d_6, hexanedioic acid–d_4, 3-hydroxy pentanedioic acid–d_5, glucose–$^{13}C_6$, and pentaerythritol–d_5. These standards span O : C ratios of 0 to 1 with a maximum of 4 hydroxyl groups per compound. The concentrations of these internal standards were chosen to match the local naturally low ambient concentrations, approximately an order of magnitude more dilute than that used in the prototype field deployment using Instrument 1.

To help evaluate sample recovery stability, we define a measure of trending in system response as the ratio of means of the internal standard response $S_{i,m/z}$ for the first half of a consistent operation period relative to the second half of that period for a given compound i with mass-to-charge ratio m/z:

$$\mathrm{Tr}_i = \frac{\sum_{n/2+1}^{n} S_{i,m/z}}{\sum_{1}^{n/2} S_{i,m/z}}. \tag{5}$$

This metric for stability was applied to data from both instruments. For Instrument 1 with two sampling periods using different sampling durations, 30 and 90 min, each period is treated separately because sample size has a strong influence on absolute compound recoveries. For Instrument 2, a period with stable operating conditions was selected, namely one between MS source cleaning, re-tuning, or system maintenance changes likely to directly affect signal response and thereby compromise the VLI evaluation.

3.4 Testing carryover in dual-cell VLI

During the development of the dual-cell instrument, tests were performed to evaluate carryover from one cell into the other, which serves as a control test of sample handling by the VLI. Incomplete delivery of one cell's sample – whether from diffusion, cold spots, dead volumes, or small leaks – can be evaluated using a cell blank of the companion cell.

To test for this potential source of cross contamination, ambient air samples in Berkeley, CA, were collected in one cell (Cell 2) for 1 h and then analyzed. Immediately following this analysis, the other cell (Cell 1) was analyzed with no sample or introduction of standards. Carryover fraction (f_{carry}) was calculated for a given ion as the detector response measured in the blank in Cell 1 and as a fraction of the sample in Cell 2 after removing background contamination in Cell 1:

$$f_{\mathrm{carry},m/z} = \frac{\sum_{t_R} \left(S_{\mathrm{blank},m/z} - S_{\mathrm{bkgd},m/z}\right)}{\sum_{t_R} S_{\mathrm{samp},m/z}}. \tag{6}$$

Detector response from an analysis of Cell 1 in the absence of sampling on either cell was considered background signal, $S_{\mathrm{bkgd},m/z}$, and subtracted from the blank to remove the fraction of detector response constantly present as background, not caused by cell-to-cell carryover. The remaining signal is assumed to have come from the analysis of the sampled cell. Signal of each mass-to-charge ratio, $S_{m/z}$, was summed across GC retention times spanning tridecane to heptacosane and compared to the analysis of the sample, $S_{\mathrm{samp},m/z}$, on the other cell (Cell 2).

4 Results

4.1 Model validation for column and vent flows

Evaluating the capillary flow model is easiest for the ambient outlet case because the column flow can be measured directly and the continuum approximation applies throughout both capillaries. For these reasons, this set of calibration data was chosen as the primary test data set with which the model was "tuned" to calculate precise capillary inner diameter (d) by maximizing agreement with the measured flows. Specifically, the measured vent flow was regressed against the modeled vent flow (i.e., Q_{cell} given by Eq. 1), and the sum of the

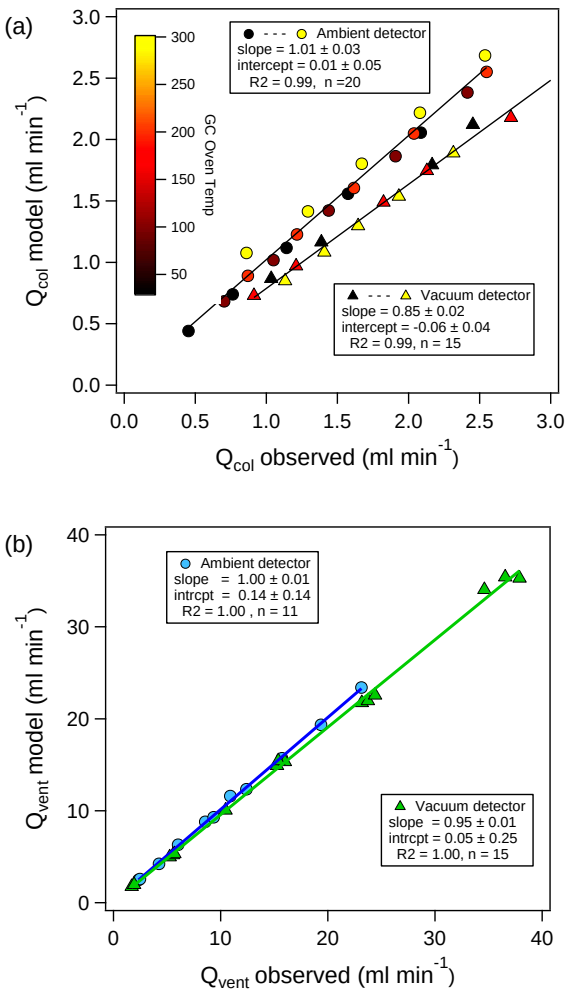

Figure 4. Model vs. measurement of average column flow **(a)** and vent outlet flow **(b)** for cases of FID (ambient)- or MS (vacuum)-based detection. For the column flow, the oven temperature (color of points) is used to adjust the helium viscosity in the flow model.

residuals was minimized by variation of the C_{cell} capillary inner diameter. Similarly, the measured column flow was regressed against the model column outlet flow, and the sum of the residuals was minimized by variation of d. The resulting optimized capillary inner diameters can be compared to the manufacturer's specifications, but differences obtained can also be attributed to other factors affecting the resulting flows (e.g., tube restrictions introduced during fabrication or application of compression fittings during assembly).

The vent and column outlet flows were measured for 20 and 11 pressure and temperature pairs, respectively, over the pressure range of 150 to 340 kPa and for column temperatures equal to 30, 100, 200, and 300 °C. The resulting fitted model was used to generate modeled flow values for each of the original data as presented in Fig. 4. Only the column flow is affected by oven temperature, indicated by symbol color in Fig. 4a, through helium viscosity changes. The resulting optimized capillary inner diameters were 0.244 mm for the column and 0.133 mm for the control capillary C_{cell}. These values are close to the manufacturer's values of 0.25 and 0.125 mm as expected given the dominance of the two capillaries in governing the resulting flows. The linear regression results for both flows indicate excellent agreement between the tuned model and the measured flows under all conditions tested:

$$\text{Column}: Q_{\text{model}} = (1.01 \pm 0.03)\, Q_{\text{meas}} + (0.01 \pm 0.05),$$
$$R^2 = 0.99[\text{Ambient case}]; \quad (7)$$
$$\text{Vent}: Q_{\text{model}} = (1.00 \pm 0.01)\, Q_{\text{meas}} + (0.14 \pm 0.14),$$
$$R^2 = 1.00[\text{Ambient case}]. \quad (8)$$

With the resulting optimized capillary inner diameters obtained for the ambient case, the vacuum outlet case can be evaluated. For this comparison, the mean column flow was measured using micro-injections of air and timed column transit times for 15 sets of conditions at three oven temperatures (80, 200, 300 °C) at each of four pressures ranging from 140 to 430 kPa. The measured vent and column flows are compared to the model results using the optimized d parameters from the ambient case. The results for the vacuum outlet case are shown in Fig. 4 (triangles) along with the model fit results:

$$\text{Column}: Q_{\text{model}} = (0.85 \pm 0.02)\, Q_{\text{meas}} - (0.06 \pm 0.04),$$
$$R^2 = 0.99[\text{Vacuum case}]; \quad (9)$$
$$\text{Vent}: Q_{\text{model}} = (0.95 \pm 0.01)\, Q_{\text{meas}} + (0.05 \pm 0.25),$$
$$R^2 = 1.00[\text{Vacuum case}]. \quad (10)$$

Both measured flows were higher than the model predicted using the ambient calibration, with the mean column flow approximately 15 % higher than the model and the measured vent flow 5 % higher than the model. The higher measured column flow may result from the non-continuum conditions that exist towards the column outlet as the pressure decreases and the mean free path of the carrier flow molecules therefore approaches the tube inner diameter. This explanation would not account for the vent flow, which depends only on P_{split} and not the state of the column flow. Better agreement could be obtained by choosing the vacuum set of data for the optimization or tuning process. Given the wide range of conditions covered in these two sets of measurements, the model is sufficiently accurate to be highly useful in the design of VLI systems for different instruments. Typically, the nominal capillary parameters presented by manufacturers are good enough to select capillary dimensions for a given set of operating conditions, and then tuning or calibrating the interface produces a more accurate control model if needed. For use in TAG instruments where the column head pressure is directly controlled and authentic standards are used to obtain absolute retention time references, the need to calibrate d for individual VLI manifolds based on a fixed geometry is unnecessary.

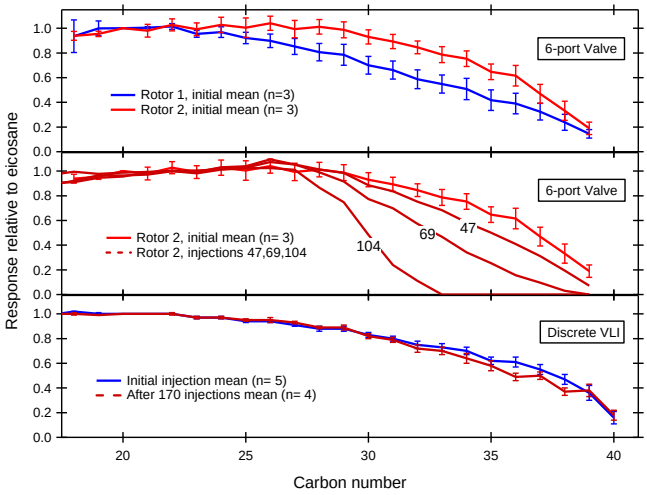

Figure 5. Average n-alkane transfer efficiency from multiple injections ($n = 3$ to 4) normalized by the peak response for n-eicosane (C_{20} alkane). **(a)** Initial performance of two rotors on the same six-port valve. **(b)** Worst-case scenario showing steady degradation in performance observed with the six-port valve shown by four injections spanning 104 consecutive injections as compared to the average initial injection. **(c)** Average initial injection and average final injection following 173 injections using the discrete prototype valveless injection system. Error bars equal ± 1 standard deviation of the mean.

4.2 Laboratory comparison to valve-based system

Degradation of sample transfer efficiency with the traditional six-port valve over time is difficult to quantify because of the lack of predictable behavior during normal operation. The lack of predictability and potential for field study interruption was the primary motivation for developing the VLI system.

Figure 5a illustrates the initial performance variability inherent with the relative transfer efficiency between two different sealing rotors on the same six-port valve. Each curve is the average of three consecutive injections for the two different rotors with ±1 standard deviation indicated by error bars. The greatest differences are observed for $> C_{25}$. The seal and transfer efficiency can last for days to weeks without significant change, but improvements in performance during continuous operation are rarely observed after the initial brief conditioning period. A rotor can fail almost immediately in a field study environment, but more often it will slowly degrade over time. For instance, the second rotor initially shows a relative recovery at C_{37} of ~ 0.5, but during the subsequent hundred injections, Fig. 5b, this level of recovery was only attained at C_{35}, C_{33}, and then C_{30} for the 47th, 69th, and 104th subsequent injection, respectively. The use of an anti-stiction coating (AMC18 treatment, AMCX) can greatly improve the longevity of the Vespel graphite rotor used to provide the high-temperature seal. Through use of this coating, a typical 2–4-week lifespan based on 24 analyses or sample injections per day can be extended by as much as a factor of 4 (B. J. Williams, personal communication, 2014). Inconsistent results even with this coating, however, are the rule.

Figure 5c demonstrates the long-term stability and inherent reliability of the prototype VLI during laboratory evaluations. The relative recovery of the same standard used for the six-port valve evaluation is shown for the beginning and end of a sequence of 173 injections during which no changes were made to the injection system. The average relative transfer efficiency is given for four repeated injections at the beginning and end of this series, with error bars equal to ±1 standard deviation for each set of injections. The initial, short-, and long-term performance equals or exceeds the performance of the six-port valve, particularly above C_{30}. Restricting a comparison to C_{22} to C_{38}, the median relative standard deviation for the six-port valve was 6 and 7 % for rotor 1 and 2, respectively, while both the initial and final median relative standard deviation for the VLI system was 2 %. During the development and testing of the dual-cell SV-TAG instrument, over 4000 successful injections were performed using just two integrated manifolds.

4.3 Application to in situ field measurements

The prototype VLI was first deployed in the TAG instrument during a 2010 California air quality study (CalNex) (Zhao et al., 2013b). During the course of 4 weeks of continuous sampling, 63 manual liquid-based internal standard injections were made on top of regular ambient samples at the average rate of 1.6 per day. Peak elution retention times for these compounds were highly stable, with standard deviations from the mean ranging from 0.8 to 1.5 s for all internal standards, including oxygenates (not shown) more volatile than n-hexatriacontane (C_{36}). These variations are an order of magnitude smaller than the typical GC peak widths exhibited by all compounds eluting with or before n-dotriacontane (C_{32}).

Peak integrals for each of 10 perdeuterated internal standards are shown as mean normalized and offset time series in Fig. 6 arranged top to bottom by decreasing volatility (increasing boiling point) with the relative standard deviation (RSD) for each compound. The compounds chosen span 16 to 28 carbon atoms, namely n-hexadecane purely in the gas phase up to n-octacosane almost fully in the particle phase. The two study periods employing different sampling durations show the same steady response. All compounds show consistent but varying levels of variability, with all saturated hydrocarbons less volatile than n-tetracosane varying from 4 to 7 % of the mean (heavy dashed lines), while compounds with decreasing volatility demonstrate increasing variations about the mean in response to matrix changes including sample size. Samples collected through the gas-phase denuder are shown with open symbols, while closed symbols indicate samples bypassing the denuder (i.e., gas + particle phase).

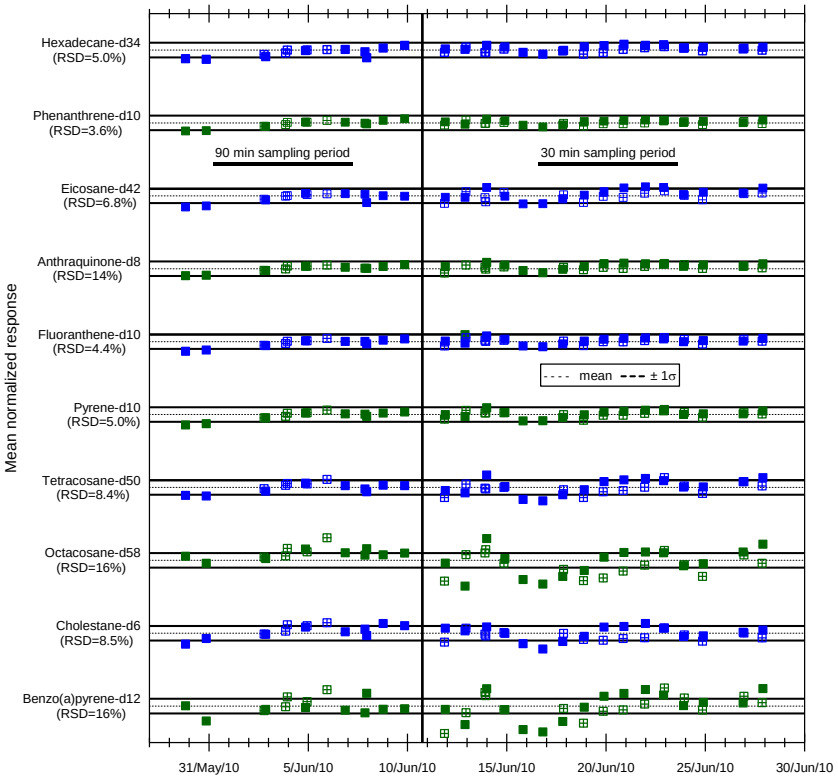

Figure 6. Field performance of prototype VLI system demonstrated by relative stability of an internal standard mix of deuterated compounds injected on top of ambient samples at the average rate of 1.6 per day. Each compound is normalized by the study mean, offset, and arranged top to bottom by decreasing volatility. Open (closed) symbols denote samples acquired with (without) a vapor-phase denuder. The least volatile compounds show some sensitivity to sample size on recovery, illustrating the need for an internal standard for quantifying compounds of similar volatility. The relative standard deviation (RSD) for each compound is given below each name, while mean and ±10 % of mean lines are added for reference.

Comparing the two study periods illustrates the role of sample size on recovery. For the first period in which sampling was conducted for 90 min, little to no effect of the denuding of the gas-phase component is detectable. For the latter period, however, in which the sampling period was reduced to 30 min to improve temporal resolution, the absence or presence of the gas-phase contribution is readily observable across all compounds but especially for *n*-tetracosane and those with lower volatility. We surmise that, with 90 min samples, sufficient particulate material is collected to reduce the effect of the vapor phase being present or not as determined by use of a carbon denuder (filed and open symbols, respectively).

The lack of any long-term trending is further evidence of long-term consistency of sample injection using the VLI system. Figure 7a and b show the ratio of first half to second half average response, the trend metric Tr given by Eq. (5), with a small positive increase in recovery for both sampling periods but no significant dependence on compound volatility. The 95 % confidence interval about the ratio mean is derived from propagating the standard deviation of the two half population means and using the t distribution for the error estimate. Taken together, these data demonstrate implicitly the lack of any long-term degradation in performance in the prototype VLI system.

With the introduction of online derivatization with Instrument 2, the VLI performance can be evaluated using a broader range of compound moieties. Using the same trend metric as above, Fig. 7c shows the resulting change in response to over 343 sample injections in the course of 19 days of uninterrupted sampling in which a total of 899 sample injections were performed for both cells. A small downward trend in recovery on the order of 2 % week^{-1} is observed that is flat and without significant carbon number or most significantly polarity (number of OH groups) dependence. This small flat reduction is most likely attributable to detector sensitivity decline and is small enough to not affect the ability to use the response of these internal standards to fully quantify the concentrations of ambient organic species, including those that are highly oxygenated.

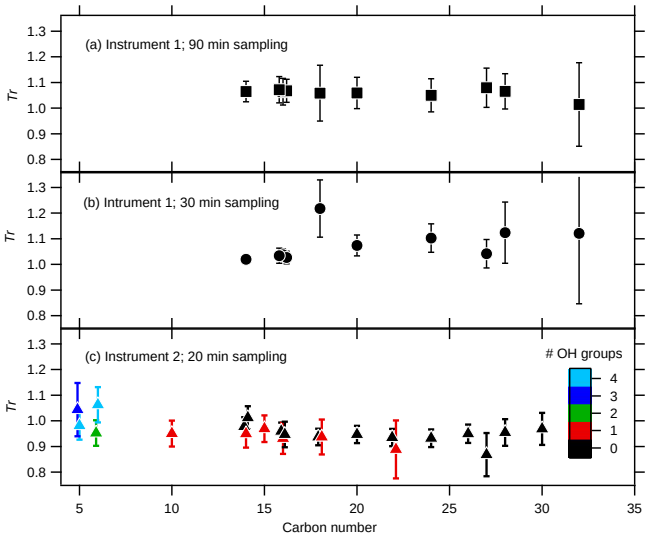

Figure 7. Stability of an internal standard recovery given by the trend metric (Tr) defined by Eq. (5) and equal to the ratio of mean response for the last half interval to that of the first half interval for individual compounds. Non-polar hydrocarbon recovery is shown for Instrument 1 with the prototype VLI for the 90 min **(a)** and 30 min **(b)** sampling periods. One cell of the dual-cell Instrument 2 sampling for 20 min is shown for a suite of compounds including highly polar compounds that are derivatized **(c)**. Vertical bars define 95 % confidence interval for Tr. Color indicates number of OH groups present before derivatization.

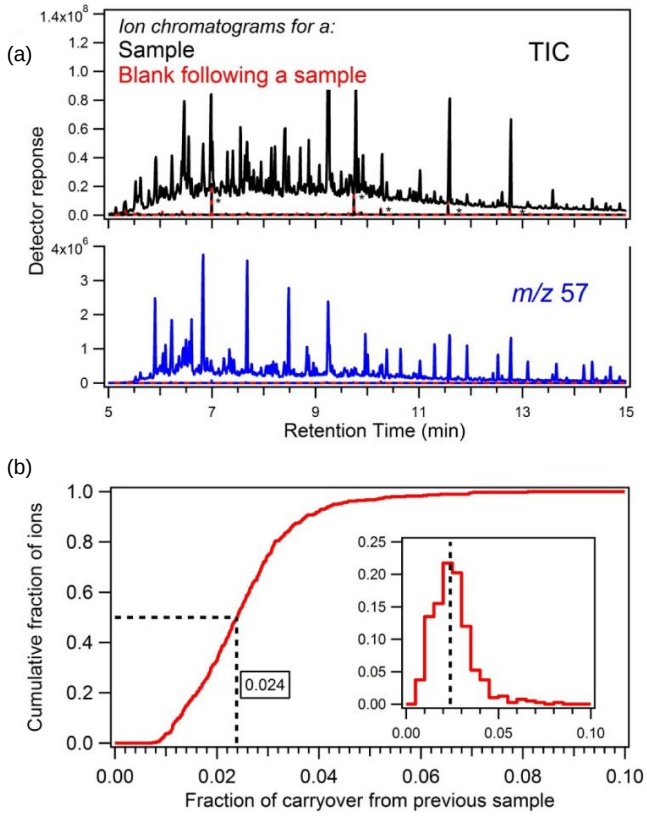

Figure 8. (a) Total ion chromatograms (black) and sample single ion chromatogram for a ubiquitous mass fragment (m/z 57, blue) for a 1 h sample of ambient air in Berkeley, CA, collected on Cell 2 (solid lines) and a cell blank of Cell 1 analyzed immediately afterward (red dashed). Starred peaks are compounds known to be present as internal contaminants. **(b)** The histogram (inset) and cumulative distribution of carryover from one cell into the other, calculated as demonstrated above: collecting sample in Cell 2, and comparing the detector response of this sample to the response of a subsequent analysis of Cell 1 which contains no sample (i.e., blue/red dashed line divided by blue line). Detector response of the 100 most abundant ions was used to measure carryover for 4 sets of 1 h Cell 2 samples followed by Cell 1 blanks ($N = 400$ mass-to-charge ratios). The median carryover from one cell into the other is 2.4 %.

4.4 Dual-cell carryover

Average cell-to-cell carryover in the dual-cell TAG system was quantified through a set of four 1 h samples of ambient air in Berkeley, CA, collected on Cell 2 followed by subsequent analyses of an empty Cell 1. An example of the resulting chromatograms for total ion abundance and the most abundant hydrocarbon ion (57 m/z) is shown in Fig. 8a, in which the background-subtracted blank on Cell 1 is shown (red dashed) with the analyzed sample on Cell 2 (solid color). Starred peaks are isolated compounds known to be present as internal contaminants that otherwise do not interfere with sample analysis. The fraction of carryover was calculated for the 100 most abundant ions or 400 individual ion measurements using Eq. (5) (i.e., blue/red dashed line divided by blue line).

Figure 8b shows the cumulative distribution of $f_{\text{carryover}}$ and its histogram (inset) demonstrating a cell-to-cell carryover of less than 4.4 % for 95 % of measured masses, with a median of 2.4 %. In addition to individual ions, total carryover was also measured using the total ion chromatogram and found to be 2.6 ± 0.1 % for the four sample sets. Further evidence of < 3 % carryover comes from a long, continuous data set of ambient measurements in which one cell collected whole-air samples while gas-phase components were removed in the other cell; in these measurements, the gas-phase fraction of a highly volatile compound, pinonic acid, was regularly measured to have a signal 2–3 % of the whole-air sample, providing a comparable upper bound for potential cell carryover.

5 Conclusions

A persistent goal for all versions of the TAG instrument is to collect continuous, hourly in situ measurements in the field over several weeks to months. It is only with this type of method that robust statistical analyses on the resulting data can be employed. Introduction of the valveless injection sys-

tem has greatly contributed to increasing the reliability of the TAG instrument, taking advantage of the collection flow rate being significantly higher than the detector flow rate. The capillary flow model was shown to be sufficiently accurate to allow designing VLI systems for a variety of applications under different operating conditions and detectors. Laboratory and field data demonstrated that this method of sample introduction provides increased long-term reliability and improved reproducibility without any trade-offs. Since its introduction in the TAG system, no VLI failures have been experienced in four separate field campaigns. Extension to a dual-cell interface was made, demonstrating less than 3 % carryover between cells that greatly facilitates a more direct measurement of gas–particle partitioning. The VLI system is highly flexible and should be able to provide improvements in reliability for other online, though not necessarily chromatography-based, instruments that employ sample concentration prior to analysis.

Appendix A: EPC flow capillary

Sample diversion at the split point (P_{split} in Fig. 1) is a concern for the case where sample species are highly diffusive relative to injection timescales and length scales. The resulting migration of these species up along the pathway towards the EPC can lead to split peak injections as the diverted sample transfers to the analytical column after the primary transferred sample has moved towards the detector. To avoid this potential sample diversion, an extra control capillary, C_{epc}, replaces the solenoid valve shown in Fig. 1b and c, inserted between the EPC and the VLI split pressure point to provide enough pressure drop to permit control of a minimum flow out of the EPC during sample injection (see Fig. A1). This constant but minor flow prevents any sample diversion during injection. The original prototype took this approach, and the modeling formulation is presented here. Although for the range of TAG analytes currently studied this approach has proven unnecessary, in the application of the VLI to gas-phase species this approach could be employed rather than resorting to cryofocusing on the analytical column to insure consolidated sample injections.

The three flows of interest for modeling the VLI in the case of the presence of C_{epc} are the column flow Q_{col}, the cell flow Q_{cell}, and the EPC flow Q_{epc}, which follow directly from Eq. (1):

$$Q_{col} = a_{col}\left(\frac{P_{split}^2 - P_{det}^2}{P_{ref}}\right)\left(\frac{T_{ref}}{T_{col}}\right), \tag{A1}$$

$$Q_{cell} = a_{cell}\left(\frac{P_{split}^2 - P_{cell}^2}{P_{ref}}\right)\left(\frac{T_{ref}}{T_1}\right), \tag{A2}$$

$$Q_{epc} = a_{epc}\left(\frac{P_{epc}^2 - P_{split}^2}{P_{ref}}\right)\left(\frac{T_{ref}}{T_2}\right), \tag{A3}$$

where we have introduced "conductance" factors a for each capillary:

$$a_{col} = \pi d_{col}^4 \Big/ 256\eta L_{col},$$
$$a_{cell} = \pi d_1^4 \Big/ 256\eta L_1,$$
$$a_{epc} = \pi d_2^4 \Big/ 256\eta L_2,$$

with the implicit understanding that the viscosities in the a factors are evaluated using Eq. (2) with their respective capillary temperatures.

During sampling and flow calibrations of the capillaries, the non-column flow exiting the split point, Q_{cell}, is equal to the sum of the flow exiting the vent plus the bleed flow into the cell. During testing the cell is sealed off and all of this flow exits the vent, where it can be conveniently measured. Whether this flow is directed entirely out the vent or split between the vent and the cell has only a minor effect on this flow even when the cell is at half an atmosphere during critical flow sampling.

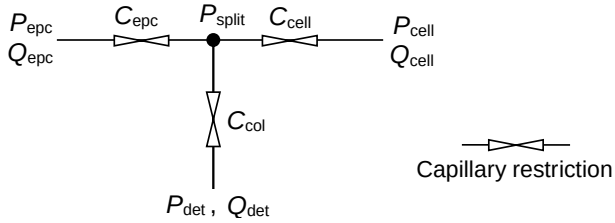

Figure A1. Simplified diagram of generalized VLI system for modification of an Agilent 6890 gas chromatograph showing the use of an extra capillary between the split point and EPC to enable flow control out of the EPC during sampling injection.

We arbitrarily define the flow to be positive in the direction leading from the EPC into the split point and then out towards the cell and through the column. By mass conservation, the EPC flow Q_{epc} equals $Q_{col} + Q_{cell}$ at the split point, so by substituting using Eqs. (A1)–(A3) and making the simplification that the two capillaries C_{epc} and C_{cell} are at the same temperature such that $T_{epc} = T_{cell} \equiv T_c$ and taking the reference pressure and temperature to be that at the split point, i.e., $(T_{ref}, P_{ref}) = (T_{split}, P_{split})$, we obtain the relationship:

$$a_{epc}\left(P_{epc}^2 - P_{split}^2\right) = a_{col}\left(P_{split}^2 - P_{det}^2\right) T_c \Big/ T_{col} + a_{cell}\left(P_{split}^2 - P_{cell}^2\right). \tag{A4}$$

Equation (A4) can be solved for P_{epc} to obtain

$$P_{epc} = \sqrt{\frac{\left(a_{epc} + a_{cell} + a_{col} T_c \Big/ T_{col}\right) P_{split}^2 - a_{col} P_{det}^2 T_c \Big/ T_{col} - a_{cell} P_{cell}^2}{a_{epc}}}. \tag{A5}$$

Equation (A5) governs the VLI operating flows during both sample injection and analysis. To express the control parameter P_{epc} as a function of flow rate, either Eq. (1) can be solved algebraically or Eq. (4) can be solved numerically for the split pressure P_{split} and substituted into Eq. (A5) for the case of either specified outlet or average column flow, respectively. During analysis, the EPC pressure is adjusted to provide the appropriate GC column head pressure P_{split}. For the VLI sample injection mode, we want to maximize the sample delivery flow rate Q_{cell} by selecting the smallest P_{epc} that maintains positive flow out of the EPC. We prevent any sample diversion away from the column by imposing the condition $P_{epc} - P_{split}$ be maintained greater than the practical resolution of the pressure controller. For the Agilent 6890 used in this work, this constraint was typically taken to be ~ 10 kPa.

Acknowledgements. Funding for this work was provided by the Department of Energy under STTR grants DE-FG02-05ER 86235 and DE-FG02-08ER86335 and SBIR grant DE-FG02-08ER85160. G. Isaacman is supported by the National Science Foundation (NSF) Graduate Research Fellowship (NSF grant: DGE 1106400).

Edited by: P. Herckes

References

Blumberg, L. M.: Temperature-Programmed Gas Chromatography, Wiley-VCH, Weinheim, Germany, 2010.

Davankov, V. A., Onuchak, L. A., Kudryashov, S. Y., and Arutyunov, Y. I.: Averaging the pressure and flow rate of the carrier gas in a gas chromatographic column, Chromatographia, 49, 449–453, 1999.

Deans, D. R.: Sample injection in gas chromatography, in: Patent, Google Patents, 1972.

Deans, D. R.: Gas flow switching method and apparatus, in: Patent, Google Patents, 1973.

Deans, D. R.: A new gas sampling device for gas chromatography, J. Chromatogr. A, 289, 43–51, 1984a.

Deans, D. R.: Sample injection, in: Patent, Google Patents, 1984b.

Giddings, J. C.: Role of Column Pressure Drop in Gas Chromatographic Resolution, Anal. Chem., 36, 741–744, 1964.

Goldstein, A. H. and Galbally, I. E.: Known and unexplored organic constituents in the earth's atmosphere, Environ. Sci. Technol., 41, 1514–1521, 2007.

Hamilton, J. F., Webb, P. J., Lewis, A. C., Hopkins, J. R., Smith, S., and Davy, P.: Partially oxidised organic components in urban aerosol using GCXGC-TOF/MS, Atmos. Chem. Phys., 4, 1279–1290, doi:10.5194/acp-4-1279-2004, 2004.

James, A. T. and Martin, A. J. P.: Gas-liquid partition chromatography: the separation and micro-estimation of volatile fatty acids from formic acid to dodecanoic acid, Biochemical J., 50, 679–690, 1952.

Isaacman, G., Kreisberg, N. M., Worton, D. R., Hering, S. V., and Goldstein, A. H.: A versatile and reproducible automatic injection system for liquid standard introduction: application to in-situ calibration, Atmos. Meas. Tech., 4, 1937–1942, doi:10.5194/amt-4-1937-2011, 2011.

Isaacman, G., Kreisberg, N. M., Yee, L. D., Worton, D. R., Chan, A. W. H., Moss, J. A., Hering, S. V., and Goldstein, A. H.: Online derivatization for hourly measurements of gas- and particle-phase semi-volatile oxygenated organic compounds by thermal desorption aerosol gas chromatography (SV-TAG), Atmos. Meas. Tech., 7, 4417–4429, doi:10.5194/amt-7-4417-2014, 2014.

Kreisberg, N. M., Hering, S. V., Williams, B. J., Worton, D. R., and Goldstein, A. H.: Quantification of Hourly Speciated Organic Compounds in Atmospheric Aerosols, Measured by an In-Situ Thermal Desorption Aerosol Gas Chromatograph (TAG), Aerosol Sci. Technol., 43, 38–52, 2009.

Kroll, J. H. and Seinfeld, J. H.: Chemistry of secondary organic aerosol: Formation and evolution of low-volatility organics in the atmosphere, Atmos. Environ., 42, 3593–3624, doi:10.1016/j.atmosenv.2008.01.003, 2008.

Lambe, A. T., Logue, J. M., Kreisberg, N. M., Hering, S. V., Worton, D. R., Goldstein, A. H., Donahue, N. M., and Robinson, A. L.: Apportioning black carbon to sources using highly time-resolved ambient measurements of organic molecular markers in Pittsburgh, Atmos. Environ., 43, 3941–3950, 2009.

Lewis, A. C., Carslaw, N., Marriott, P. J., Kinghorn, R. M., Morrison, P., Lee, A. L., Bartle, K. D., and Pilling, M. J.: A larger pool of ozone-forming carbon compounds in urban atmospheres, Nature, 405, 778–781, 2000.

Lide, D. R.: CRC Handbook of Chemistry and Physics: A Ready-reference Book of Chemical and Physical Data, Book, Whole, CRC Press, 1991.

McNair, H. M. and Miller, J. M.: Basic gas chromatography, John Wiley & Sons, 2011.

Ras, M. R., Borrull, F., and Marcé, R. M.: Sampling and preconcentration techniques for determination of volatile organic compounds in air samples, TrAC-Trend. Anal. Chem., 28, 347–361, 2009.

Robinson, A. L., Donahue, N. M., Shrivastava, M. K., Weitkamp, E. A., Sage, A. M., Grieshop, A. P., Lane, T. E., Pierce, J. R., and Pandis, S. N.: Rethinking organic aerosols: Semivolatile emissions and photochemical aging, Science, 315, 1259–1262, 2007.

Williams, B. J., Goldstein, A. H., Kreisberg, N. M., and Hering, S. V.: An in-situ instrument for speciated organic composition of atmospheric aerosols: Thermal Desorption Aerosol GC/MS-FID (TAG), Aerosol Sci. Technol., 40, 627–638, 2006.

Williams, B. J., Jayne, J. T., Lambe, A. T., Hohaus, T., Kimmel, J. R., Sueper, D., Brooks, W., Williams, L. R., Trimborn, A. M., and Martinez, R. E.: The First Combined Thermal Desorption Aerosol Gas Chromatograph-Aerosol Mass Spectrometer (TAG-AMS), Aerosol Sci. Technol., 48, 358–370, 2014.

Worton, D. R., Kreisberg, N. M., Isaacman, G., Teng, A. P., McNeish, C., Górecki, T., Hering, S. V., and Goldstein, A. H.: Thermal Desorption Comprehensive Two-Dimensional Gas Chromatography: An Improved Instrument for In-Situ Speciated Measurements of Organic Aerosols, Aerosol Sci. Technol., 46, 380–393, 2012.

Zhao, Y., Kreisberg, N. M., Worton, D. R., Teng, A. P., Hering, S. V., and Goldstein, A. H.: Development of an In Situ Thermal Desorption Gas Chromatography Instrument for Quantifying Atmospheric Semi-Volatile Organic Compounds, Aerosol Sci. Technol., 47, 258–266, 2013a.

Zhao, Y., Kreisberg, N. M., Worton, D. R., Isaacman, G., Weber, R. J., Liu, S., Day, D. A., Russell, L. M., Markovic, M. Z., and VandenBoer, T. C.: Insights into secondary organic aerosol formation mechanisms from measured gas/particle partitioning of specific organic tracer compounds, Environ. Sci. Technol., 47, 3781–3787, 2013b.